Supplemental Online Content

Kim S, Ollinger J, Song C, et al. White matter alterations in military service members with remote mild traumatic brain injury. *JAMA Netw Open.* 2024;7(4):e248121. doi:10.1001/jamanetworkopen.2024.8121

This supplemental material has been provided by the authors to give readers additional information about their work.

eMethods.

Diagnosis of TBI

Diagnosis of TBI was based on information gathered via medical record review and a comprehensive lifetime TBI history interview completed by a Masters- or PhD-level clinical research personnel who were trained to evaluate the presence and severity of TBI. The TBI history interview consisted of the Ohio State University TBI identification method.[1] Final determination and classification of TBI severity was undertaken by consensus, giving consideration to all information, during case conferencing with the interviewer and a clinician/scientist trained in neuropsychology and TBI.

MRI acquisition.

Whole-brain diffusion MRI was performed using combined Simultaneous Multislice (SMS, factor=3) and in-plane Parallel (acceleration factor=2) single-shot echo planar pulse sequence using 270 diffusion-encoding directions, acquired at b = 1000, 2000, and 3000 s/mm^2, and eighteen acquisitions at b = 0 s/mm^2 with 1.7-mm isotropic voxels. A sparse and optimal acquisition design[2] was applied to optimize the diffusion measurements in each shell and maximum uniformity of diffusion measurement directions for diffusion MRI multiple-shell acquisition. Two dMRI sets were acquired using blip-up and down phase-encoding acquisition approach. Sagittal three-dimensional (3D) inversion recovery fast spoiled gradient recalled echo T1-weighted were acquired with BRAVO sequence. T2*-weighted images were acquired using sagittal 3D gradient echo sequence.

Preprocessing of dMRI data included dMRI de-noising, Gibbs ringing removal and correction of motion and eddy current artifacts using software from the TORTOISE toolkits.[3] Susceptibility-induced off-resonance fields were estimated using the different phase-encoded images, and an undistorted structural T2-weighted MRI image was aligned to the AC-PC plane

using the HCP Preprocessing Pipeline (https://github.com/Washington-University/HCPpipelines) and used to improve registration accuracy. EPI geometric distortion correction was performed using pairs of diffusion data sets acquired with opposite phase encoding (blip-up and blip-down acquisitions).[4] dMRI images were finally upsampled to an isotropic voxel size of 1.0 mm^3, and two sets of dMRI were averaged. The b-matrices were rotated accordingly. Framewise Displacement (FD) was measured using the implementation in Nipype (https://nipype.readthedocs.io/en/latest/), following the definitions by, wherein all position measures were differentiated in dMRI volume frames by backwards differences, rotational measures were converted to arc displacement at 5 cm radius, and the sum of the absolute value of these measures was calculated.[5]

Statistical Analyses

Permutation inference Generalized Linear Model

Specifically, GLM generalized the ordinary least squares (OLS) by allowing Chi-Square distribution of the residuals, and optimized the likelihood function by allowing a t-test based on an estimated error of the coefficients. Permutation inference GLMs applied OLS with covariates of age and FD to examine the relationship between the DTI/NODDI metrics and neuropsychiatric symptoms.

To assess goodness-of-fit, likelihood ratio test (LRT) statistic, comparing the log likelihoods between the null and the full models, and R-squared static, representing the percentage of variation of diffusion metrics explained by the independent variables, were calculated.

The nonparametric statistical test was performed in the following way[6]:

(1) Collect the trials of the two experimental conditions in a single set.

(2) Randomly draw as many trials from this combined data set as there were trials in condition 1 and place those trials into subset 1. Place the remaining trials in subset 2. The result of this procedure was called a random partition.

(3) Calculate the test statistic on this random partition.

(4) Repeat steps 2 and 3 a large number of times and constructed a histogram of the test statistics.

(5) From the test statistic that was actually observed and the histogram in step 4, calculated the proportion of random partitions that resulted in a larger test statistic than the observed one. This proportion was called the *p*-value.

(6) If the *p*-value was smaller than the critical alpha-level, e.g. 0.05, then concluded that the data in the two experimental conditions were significantly different.

Calculate the Monte Carlo p-values

The Monte Carlo estimate, the Monte Carlo *p*-values, were obtained by repeating steps 2 and 3 above at 5000 times followed by comparing these random test statistics (i.e., draws from the permutation distribution) with the observed test statistic. The Monte Carlo estimate of the permutation *p*-value is the proportion of random partitions in which the observed test statistic was larger than the value drawn from the permutation distribution. Because the Monte Carlo *p*-value has a binomial distribution, its accuracy can be quantified by means of the confidence interval for a binomial proportion.[7]

Sensitivity analysis

Residual sum of squares *and* R-squared, as well as the F values (the ratio of variances of the full and the reduced OLS models) were computed and compared between the full and the reduced OLS models. We computes the Standardized Regression Coefficients (SRC) which are the normalized linear regression coefficients, and Johnson indices which allocate a share of R^2

to each input based on the relative weight allocation (RWA) system, in the case of dependent or correlated inputs.

Receiver operating characteristic (ROC) curve analysis

Dichotomus ROC curve analysis was employed to compare diffusion metrics and differentiate mTBI patients from controls based on the WM microstructural differences identified by DTI/NODDI metrics. The area under each ROC curve (AUC) was calculated to determine the optimal discriminative performance among DTI/NODDI diffusion metrics, along with PCL-C scores. The threshold value for a significant diffusion metric to distinguish mTBI patients from healthy controls was identified by maximizing the Youden index.[8]

eAppendix. ROC Curve Analysis

In the ROC curve analysis, the area under the curve (AUC) was calculated to evaluate the performance of different variables in distinguishing between mTBI and control subjects. ROC curves were generated from PCL-C total and sub-scores, as well as the significantly different DTI/NODDI ROI and TBSS clusters. PCL-C total score had the highest AUC of 0.981 ($p<.001$), followed by PCL-C D hyperarousal sub-score (AUC=0.980, $p<.001$), PCL-C C avoidance sub-score (AUC=0.960, $p<.001$), and PCL-C B re-experiencing sub-score (AUC=0.905, $p<.001$) **(eFigure 1 and eTable 4)**. For PCL-C total score, the optimal cutoff value was 23.0 with a sensitivity of 96.9% and a specificity of 87.9%.

eFigure. ROC curves of PCL-C Scores and NODDI/DTI metrics classifying mTBI from control

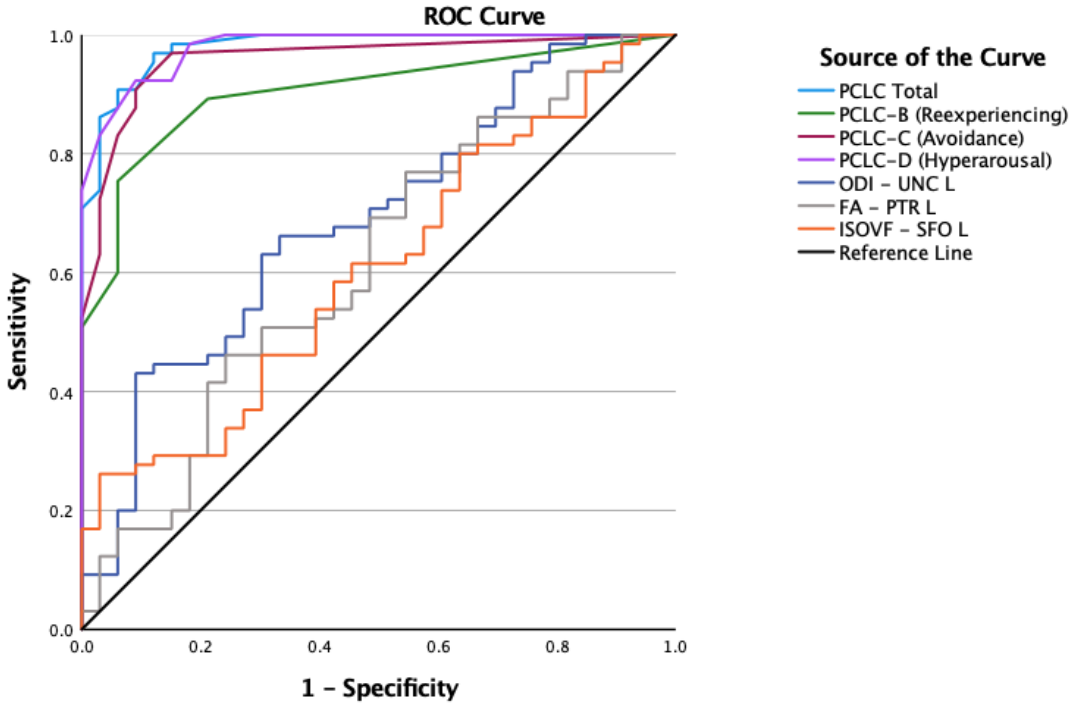

eFigure. ROC curves of PCL-C Scores and NODDI/DTI metrics classifying mTBI from control. PCL-C total and sub scores as well as neuroimaging metrics with the highest AUC values were included in the graph. PCL-C total score had the highest AUC of 0.981 (p<.001); the optimal cutoff value was 23.0 with a sensitivity of 96.9% and a specificity of 87.9%. Among all imaging metrics, ODI of the ROI UNC-L had the highest AUC of 0.698 (p=.001); the optimal cutoff value was 0.0852 with a sensitivity of 43.0% and specificity of 90.3%.

eTable 1. Index of ROIs From the JHU-ICBM-DTI-81 WM Labels Atlas

1. GCC - Genu of Corpus Callosum	23. SCR-R - Superior Corona Radiata Right
2. BCC - Body of Corpus Callosum	24. SCR-L - Superior Corona Radiata Left
3. SCC - Splenium of Corpus Callosum	25. PCR-R - Posterior Corona Radiata Right
4. FX - Fornix	26. PCR-L - Posterior Corona Radiata Left
5. CST-R - Corticospinal Tract Right	27. PTR-R - Posterior Thalamic Radiation Right
6. CST-L - Corticospinal Tract Left	28. PTR-L - Posterior Thalamic Radiation Left
7. ML-R - Middle Cerebellar Peduncle Right	29. SS-R - Sagittal Stratum Right
8. ML-L - Middle Cerebellar Peduncle Left	30. SS-L - Sagittal Stratum Left
9. ICP-R - Inferior Cerebellar Peduncle Right	31. EC-R - External Capsule Right
10. ICP-L - Inferior Cerebellar Peduncle Left	32. EC-L - External Capsule Left
11. SCP-R - Superior Cerebellar Peduncle Right	33. CGC-R - Cingulum Cingulate Gyrus Right
12. SCP-L - Superior Cerebellar Peduncle Left	34. CGC-L - Cingulum Cingulate Gyrus Left
13. CP-R - Cerebral Peduncle Right	35. CGH-R - Cingulum Hippocampus Right
14. CP-L - Cerebral Peduncle Left	36. CGH-L - Cingulum Hippocampus Left
15. ALIC-R - Anterior Limb of Internal Capsule Right	37. FX/ST-R - Fornix (crus)/Stria terminalis Right
16. ALIC-L - Anterior Limb of Internal Capsule Left	38. FX/ST-L - Fornix (crus)/Stria terminalis Left
17. PLIC-R - Posterior Limb of Internal Capsule Right	39. SLF-R - Superior Longitudinal Fasciculus Right
18. PLIC-L - Posterior Limb of Internal Capsule Left	40. SLF-L - Superior Longitudinal Fasciculus Left
19. RLIC-R - Retrolenticular Part of Internal Capsule Right	41. SFO-R - Superior fronto-occipital fasciculus Right 42. SFO-L - Superior fronto-occipital fasciculus Left
20. RLIC-L - Retrolenticular Part of Internal Capsule Left	43. IFO-R - Inferior Fronto-Occipital Fasciculus Right 44. IFO-L - Inferior Fronto-Occipital Fasciculus Left
21. ACR-R - Anterior Corona Radiata Right	45. UNC-R - Uncinate Fasciculus Right
22. ACR-L - Anterior Corona Radiata Left	46. UNC-L - Uncinate Fasciculus Left

eTable 2. Severity Ratings of GAD-7 and PHQ-9

GAD-7 Rating	Frequency	Percent
Severe	20	30.8
Moderately Severe	20	30.8
Moderate	18	27.7
Mild	5	7.7
None	2	3.1
Total	65	100.0
PHQ-9 Rating	**Frequency**	**Percent**
Severe	4	6.3
Moderately Severe	6	9.4
Moderate	25	39.1
Mild	21	32.8
None	1	1.6
Total	64	100.0

eTable 3. Results of Sensitivity Analysis of Regression Models (TBI only, n=65)

Full model: L FA UNC ~ NSI Cognitive + Age + Mean Displacement **Reduced model: L FA UNC ~ Age + Mean Displacement**				
Model	***SRC***	***Johnson Indices***	***F-Value ANOVA (Full model, Reduced model)***	***P-Value ANOVA (Full model, Reduced model)***
NSI Cognitive	0.335	0.091	7.96	0.006
Age	0.095	0.003		
Mean displacement	-0.332	0.085		
Full model: ISOVF GCC ~ PCLC Total + Age + Mean Displacement **Reduced model: ISOVF GCC ~ Age + Mean Displacement**				
Model	***SRC***	***Johnson Indices***	***F-Value ANOVA (Full model, Reduced model)***	***P-Value ANOVA (Full model, Reduced model)***
PCLC Total	0.266	0.067	4.63	*0.03*
Age	-0.051	0.004		
Mean displacement	-0.098	0.008		
Full model: L ODI FX ST ~ PCLC-C + Age + Mean Displacement **Reduced model: L ODI FX ST ~ Age + Mean Displacement**				
Model	***SRC***	***Johnson Indices***	***F-Value ANOVA (Full model, Reduced model)***	***P-Value ANOVA (Full model, Reduced model)***
PCLC-C	1.000	0.867	4.35	*0.04*
Age	6.85e-17	0.074		
Mean displacement	2.40e-16	0.059		

Table 4. Diagnostic Sensitivity and Specificity of PCL-C Scores and Diffusion Parameters for Classifying mTBI From Control

Test Result Variable(s)	AUC (95% CI)	SE	P-value	Max YI	Cutoff value	Sensitivity	Specificity
PCL-C Total	0.980 (0.961 to 1.000)	0.011	<.001	0.848	23.0	0.97	0.88
PCL-C D (Hyperarousal)	0.979 (0.962 to 1.000)	0.011	<.001	0.693	6.50	0.75	0.94
PCL-C C (Avoidance)	0.959 (0.920 to 0.998)	0.020	<.001	0.818	7.50	0.97	0.85
PCL-C B (Reexperiencing)	0.904 (0.843 to 0.964)	0.031	<.001	0.832	9.50	0.92	0.91
ODI: UNC-L	0.689 (0.579 to 0.799)	0.056	.002	0.340	0.0852	0.43	0.91
FA: PTR-L	0.615 (0.496 to 0.735)	0.061	.06	0.224	0.6210	0.77	0.45
ISOVF: SFO-L	0.605 (0.490 to 0.720)	0.059	.09	0.231	0.0652	0.26	0.97
MD: FX	0.435 (0.304 to 0.566)	0.067	.3	0.151	0.0009	0.97	0.18
RD: FX	0.429 (0.297 to 0.561)	0.068	.3	0.151	0.0006	0.94	0.21
ODI: ICP-R	0.407 (0.284 to 0.531)	0.063	.1	0.028	0.1113	0.88	0.15
ISOVF: FX	0.394 (0.267 to 0.521)	0.065	.09	0.090	0.1882	0.97	0.12
ODI: FX	0.388 (0.260 to 0.516)	0.065	.07	0.075	0.0627	0.92	0.15
ISOVF: CP-R	0.386 (0.264 to 0.509)	0.062	.07	0.000	0.0000	1.00	0.00
ODI: SCP-L	0.385 (0.263 to 0.507)	0.062	.06	0.015	0.0564	0.98	0.03
ODI: CST-R	0.383 (0.264 to 0.502)	0.061	.06	0.015	0.0625	0.98	0.03
ICSVF: CST-L	0.382 (0.261 to 0.502)	0.062	.06	0.015	0.8284	0.02	1.00
FA: UNC-L	0.380 (0.262 to 0.499)	0.060	.05	0.000	0.0000	1.00	0.00
ODI: PTR-L	0.370 (0.246 to 0.494)	0.063	.04	0.029	0.0516	0.94	0.09
ODI: FX/ST-L	0.369 (0.256 to 0.483)	0.058	.04	0.046	0.2058	0.05	1.00
ICVF: CST-R	0.348 (0.232 to 0.464)	0.059	.01	0.000	0.0000	1.00	0.00
ISOVF: GCC	0.333 (0.225 to 0.441)	0.055	.007	0.015	0.1736	0.02	1.00
ISOVF: SCC	0.332 (0.208 to 0.457)	0.064	.007	0.075	0.0690	0.92	0.15
ISOVF: BCC	0.317 (0.206 to 0.428)	0.056	.003	0.047	0.1050	0.08	0.97

*Refer to eTable 1 in Supplementary for the definition of acronyms in the JHU-ICBM-DTI-81 WM labels atlas, an expanded description of each measurement and interpretation of each measurement as they relate to TBI.

Abbreviations: AUC = Area under the curve, CI = Confidence Interval, mTBI = mild traumatic brain injury, PCL-C = PTSD Checklist – Civilian Version, SE = Standard Error, YI = Youden Index.

eReferences.

1. Corrigan JD, Bogner J. Initial reliability and validity of the Ohio State University TBI identification method. *The Journal of head trauma rehabilitation*. 2007;22(6):318-329.
2. Koay CG, Özarslan E, Johnson KM, Meyerand ME. Sparse and optimal acquisition design for diffusion MRI and beyond. *Medical physics*. 2012;39(5):2499-2511.
3. Pierpaoli C, Walker L, Irfanoglu MO, et al. TORTOISE: an integrated software package for processing of diffusion MRI data. Stockholm; 2010:
4. Irfanoglu MO, Modi P, Nayak A, Hutchinson EB, Sarlls J, Pierpaoli C. DR-BUDDI (Diffeomorphic Registration for Blip-Up blip-Down Diffusion Imaging) method for correcting echo planar imaging distortions. *Neuroimage*. 2015;106:284-299.
5. Power JD, Mitra A, Laumann TO, Snyder AZ, Schlaggar BL, Petersen SE. Methods to detect, characterize, and remove motion artifact in resting state fMRI. *Neuroimage*. 2014;84:320-341.
6. Maris E, Oostenveld R. Nonparametric statistical testing of EEG-and MEG-data. *Journal of neuroscience methods*. 2007;164(1):177-190.
7. Ernst MD. Permutation methods: a basis for exact inference. *Statistical Science*. 2004:676-685.
8. Fluss R, Faraggi D, Reiser B. Estimation of the Youden Index and its associated cutoff point. *Biometrical Journal: Journal of Mathematical Methods in Biosciences*. 2005;47(4):458-472.